Research Square

Preprints are preliminary reports that have not undergone peer review.
They should not be considered conclusive, used to inform clinical practice,
or referenced by the media as validated information.

Multi-Omics Analysis Reveals Molecular Responses of Alkaloid Content Variations in Lycoris radiata Across Different Locations

Qing-zhu Li
Shanghai Academy of Agricultural Sciences
Hong-fei Li
Nanjing Forestry University
Shi-yu Huang
Nanjing Forestry University
Jun-xu Xu
Shanghai Academy of Agricultural Sciences
Lin Zhou
Shanghai Academy of Agricultural Sciences
Zi-ming Ren
Zhen Wang
Shanghai Academy of Agricultural Sciences
Zhen Yang
Shanghai Academy of Agricultural Sciences
Xuan-min Guang
You-ming Cai
Shanghai Academy of Agricultural Sciences
Fu-yuan Zhu
Nanjing Forestry University
Liu-yan Yang
Shanghai Academy of Agricultural Sciences
Yong-chun Zhang
18913787282@163.com

Shanghai Academy of Agricultural Sciences

Research Article

Keywords: Lycoris radiata, multi-omics, soil microbiome, specialized metabolism, environmental drivers

Posted Date: September 8th, 2026

DOI: https://doi.org/10.21203/rs.3.rs-10358926/v1

License: This work is licensed under a Creative Commons Attribution 4.0 International License.
Read Full License

Additional Declarations: No competing interests reported.

Abstract

The Amaryllidaceae geophyte *Lycoris radiata* is a primary botanical source of high-value medicinal alkaloids, including the Alzheimer's therapeutic galanthamine. However, the accumulation of these compounds exhibits immense spatial and geographical variation. To elucidate the regulatory networks driving this divergence, we investigated three geographically distinct ecotypes (Hubei, HB; Guangxi, GX; Yunnan, YN) using an integrative multi-omics approach. Untargeted metabolomics revealed highly region-specific accumulation patterns of key alkaloids, such as galanthamine and lycorine. Interestingly, transcriptomic profiling uncovered a regional paradox: the Yunnan population exhibited the highest expression of core alkaloid biosynthetic genes despite possessing relatively lower target alkaloid contents, suggesting the involvement of post-transcriptional or environmental regulation. Furthermore, 16S and ITS amplicon sequencing of the rhizosphere revealed distinctly partitioned bacterial and fungal communities across regions, with the Yunnan ecotype exhibiting reduced diversity and highly specialized microbial taxa. Integrating these multi-omics datasets with 32 soil physicochemical indices demonstrated that trace metals and soil pH strongly correlated with local microbiome assembly. Mantel tests revealed that the environmental factors associated with the transcriptional activation of alkaloid biosynthetic genes were largely uncoupled from the factors correlating with terminal metabolite accumulation. Overall, this study details the profound region-specific transcriptomic, metabolomic, and micro-ecological variations in *L. radiata*, highlighting a complex environmental decoupling between genetic potential and final alkaloid accumulation.

1. Introduction

Geophytes are plants characterized by their reliance on subterranean storage organs such as bulbs, corms, or tubers to survive periods of seasonal dormancy and harsh environmental conditions (Kumari et al., 2024). Because these underground organs serve as crucial, nutrient-dense reservoirs, they are highly vulnerable to herbivores and pathogens. Consequently, geophytes have evolved sophisticated biological functions, most notably the production of potent defensive phytochemicals(Curtis, Curtis, & Miller, 2009; Rasmann & Agrawal, 2008). Within this context, the bulbs of the *Amaryllidaceae* family are exceptionally notable, as they serve as rich biochemical factories for Amaryllidaceae alkaloids, a unique class of specialized secondary metabolites that act as the plant's primary chemical shield (Liyanage et al., 2025; Mehta, Meng, Zare, Kamenetsky-Goldstein, & Sattely, 2024). *Lycoris radiata*, commonly known as the Red Spider Lily, belongs to *Amaryllidaceae*. While it is widely cultivated globally for its inflorescences and exceptional ornamental value in landscape architecture, *L. radiata* also harbors robust alkaloid biosynthesis (Chen et al., 2025). *L. radiata* yields high-value medicinal compounds, particularly galanthamine, a globally prescribed acetylcholinesterase inhibitor for Alzheimer's disease(Mucke, 2015), alongside lycorine and lycorenine, which exhibit potent antiviral and antineoplastic properties (Chen et al., 2025). Therefore, understanding and harnessing the natural biosynthetic capacity of *L. radiata* is of immense pharmaceutical importance.

Alkaloid biosynthesis in plants is a complex process. Elucidating the biosynthetic pathways of these valuable alkaloids is notoriously challenging due to the intricate, multi-step enzymatic cascades and stereochemical complexity involved(Ziegler & Facchini, 2008). Only recently have advanced analytical techniques begun to untangle these regulatory networks, with two landmark studies unveiling critical missing links in complex alkaloid biosynthesis. The elusive enzymes responsible for assembling the complex spiro-cyclic and quinoline scaffolds in plants were identified by integrated single-nucleus RNA sequencing and functional in planta assays (Lombe et al., 2026). A breakthrough study identified a complete suite of genes responsible for Amaryllidaceae alkaloid biosynthesis in geophytes like daffodils (Mehta et al., 2024). The researchers demonstrated how a core enzymatic cascade diversifies a simple, common precursor via highly specific oxidative couplings and subsequent, slightly altered chemical transformations into structurally distinct defense metabolites, including galanthamine. Apart from these genetic blueprints that represent the plants' internal capacity, the biosynthesis of alkaloids is highly plastic, multi-factor biological process profoundly regulated by external environments (Borges, Minatel, Gomez-Gomez, & Lima, 2017). Abiotic factors such as drought and water deficit have been shown to directly dictate alkaloid accumulation in *Lycoris aurea* and *Chelidonium majus* (Liang et al., 2020; Yahyazadeh, Meinen, Hänsch, Abouzeid, & Selmar, 2018). Biotic factors such as specialized root-associated bacteria concurrently evolve specific genes to catabolize and alter the toxic plant glycoalkaloids while plant roots secrete specific defensive alkaloids to actively modulate the assembly of the surrounding bacterial communities (Nakayasu et al., 2021; Nakayasu et al., 2023; Pang et al., 2021; Sasse, Martinoia, & Northen, 2018).

To decipher the complex biological mechanisms of the *Lycoris* genus, researchers have relied on single-omic or foundational comparative omics approaches(Z.-M. Ren et al., 2022). Genomic and karyotypic profiling were employed to trace the evolutionary lineage and natural hybridization of the genus (Quan et al., 2024; Z. Ren et al., 2026; Shu et al., 2025). Isolated proteomic analyses have been utilized to investigate the molecular mechanisms governing development and flowering in *L. radiata* (Jiang, Chen, Wei, & Cai, 2021), as well as to identify key metabolic enzymes such as *O*-methyltransferase (OMT) and *N*-methyltransferase (NMT) that drive alkaloid variations among different *Lycoris* species (Tang et al., 2023). Furthermore, transcriptomic and metabolic profiling in *L. radiata* has successfully identified core galanthamine biosynthetic genes such as phenylalanine ammonia lyase (PAL) and cytochrome P450 enzymes (CYP96T1), and mapped their tissue-specific expression (Chang H. Park et al., 2019). While these targeted studies have successfully identified physiological responses and internal genetic clusters, gene or protein expression levels alone frequently do not correlate linearly with final content in wild environments (Fernie & Stitt, 2012). Consequently, integrative multi-omics has emerged as a substantially more powerful tool for dissecting complex, multi-factor biological systems. The simultaneous integration of transcriptomic, metabolomic, and environmental datasets of he related species *Lycoris aurea* successfully mapped the interactive networks between specific soil properties, microbial communities, and alkaloid production (Zuo et al., 2024), suggesting the possibility to unveil both the internal genetic regulators and the external environmental drivers that dictate the complex biosynthesis of alkaloids in *L. radiata*.

In our study, we identified massive regional variations of *L. radiata* on certain natural alkaloid content. To understand the specific molecular and ecological mechanisms driving the regional variations, we conducted an integrative, multi-omics investigation of *L. radiata* populations across three highly divergent geographical habitats in China (Hubei, Guangxi, and Yunnan). We aimed to characterize the localized micro-environments by profiling the rhizosphere microbiomes via 16S and ITS amplicon sequencing and quantifying 32 physicochemical soil indices. By integrating these complex environmental datasets with transcriptomics and untargeted metabolomics, this study seeks to identify the specific edaphic and microbial factors that correlate with key bioaccumulation and, thereby unravelling the multi-factor regulatory networks responsible for the spatial heterogeneity of alkaloid accumulation, and providing a critical theoretical foundation for the targeted agricultural cultivation of this invaluable medicinal resource.

2. Materials and methods

2.1 Site Description

We investigated the distribution of the *L.radiata* across 11 major provinces in China (Figure 1A), selecting Xingshan County in Yichang City, Hubei Province (110°45', 31°14', Group HB), Zhenxiong County in Zhaotong City, Yunnan Province (104°18', 27°17', Group YN), Yanling Couty in Zhuzhou City, Hunan Province (113°46', 26°29', Group HN) and Dumo County in Guilin City, Guangxi Province (110°06', 24°16', Group GX) for an in-depth comparative study. Xingshan County features a subtropical monsoon climate, with an average temperature of 15 °C and an annual rainfall of 1100 mm, recording the highest and lowest annual temperatures at 43 °C and -9 °C, respectively. Most areas in Zhenxiong County have a warm temperate monsoon mountain climate with distinct four seasons: late spring, short summer, early autumn, and long winter. The annual average temperature was 13 °C, recording the highest and lowest annual temperatures at 34 °C and -5 °C, respectively, the annual rainfall was 840 mm. Dumo County belongs to the subtropical monsoon climate, with high temperatures and heavy rainfall in summer and mild and little rainfall in winter. This climate characteristic makes the weather changes in Dumo Town more obvious, with hot and humid summers and relatively mild winters. The annual average temperature was 19 °C, recording the highest and lowest annual temperatures at 34 °C and 8 °C, respectively, the annual rainfall was 2000 mm.

2.2 Plant and Soil Sampling

All collected plant specimens were collected in November 2024 by Dr. Junxu Xu from Shanghai Academy of Agricultural Sciences formally and identified as *Lycoris radiata* by Prof. Pengchong Zhang from Hangzhou Botanical Garden. Voucher specimens representing the 11 wild populations were deposited in the Hangzhou Botanical Garden, under voucher accession numbers HB: HZ077449, SX: HZ077450, ZJ: HZ077451, CQ: HZ077452, JX: HZ077453, SC: HZ077454, GZ: HZ077455, SD: HZ077456, GX: HZ077457, YN: HZ077458 and HN: HZ077459, respectively. The voucher numbers correspond to the 11 sampling locations as shown in Figure 1. Five sets of plant bulb samples (each with three biological replicates)

were obtained from the three specified locations, denoted as HB, YN and GX. These samples were utilized to analyze alkaloid content, conduct RNA-seq and metabolome analysis. Concurrently, rhizosphere soil samples were procured from these three locations using a serpentine five-point sampling technique after the initial removal of surface litter and fallen branches. Soil samples were preserved in self-sealing bags for subsequent processing. Soil samples were dried in an oven at 105 °C to ascertain their dry weight.

The collection and use of the wild plant materials complied with all relevant institutional, local, and national guidelines and legislation. All plant materials were collected and analyzed within China, and no specimens or plant materials were imported or exported during this study.

2.3 Plant and Soil Properties

The physicochemical properties of the rhizosphere soil were primarily measured including water content (WC), pH, total nitrogen (TN), organic matter (OM), total phosphorus (TP), total potassium (TK), available nitrogen (AN) and selenium (Se). The fresh soil sample was accurately weighed and baked for 12 h in an oven preheated to 105 °C. Subsequently, the treated soil sample was moved into a dryer to cool to room temperature (30 min) and weighed immediately to calculate soil WC. For soil pH determination, a total of 10 g soil sample was passed through a 1 mm sieve and then added with 25 mL distilled water. The above solution was allowed to stand for 30 min, and the suspension was measured for pH with a PH metre (PHS-2F). Soil nutrients were measured as described previously by Bao (2000). Briefly, soil carbon and nitrogen levels were analyzed with an elemental analyzer (MACRO, Elementar, Germany). Flame photometry was employed to measure TK, and TP was determined via the molybdenum antimony anti-colorimetric method. AN was assessed through sodium hydroxide hydrolysis followed by the Kjeldahl nitrogen determination method, and Se was measured using atomic fluorescence spectroscopy.

2.4 Ultra Performance Liquid Chromatography Tandem Mass Spectrometry (UPLC-MS/MS) Analysis

Galanthamine (Gal), Lycoramine (Lycm), and Lycorine (Lyc) were purchased from Shanghai TCI Development Co., Ltd., and characterized as described previously (Li et al., 2018; Li et al., 2021). Plants from each group were randomly selected, chopped and mixed well. The content of three alkaloids was determined using LC-MS/MS method. Briefly, about 0.02 g of freeze-dried samples were extracted by ultrasonication in 2 ml of 70 % HPLC grade ethanol. The mixture was then centrifuged at 12,000 rpm for 10 min to obtain supernatants that were then vacuum-dried and re-dissolved in 1 mL of 0.1 % formic acid-acetonitrile (V/V = 95/5) for LC-MS/MS analysis. The analysis and separation conditions were the same as we have described elsewhere (Li Q. et al., 2021). The transition reactions 288→231, 290→189, 288→147 (m/z) were used to quantify Gal, Lycm, and Lyc, respectively. Experiments were conducted with three independent biological replicates.

2.5 RNA Sequencing

The ethanol precipitation protocol and CTAB-pBIOZOL were used to purify the total RNA according to the manufacturer's instructions. Subsequently, the total RNA was identified and quantified using a Qubit fluorescence quantifier ((Thermo Fisher Scientific, Waltham, USA)) and a Qsep400 high-throughput biofragment analyzer (Bioptic Inc, Jiangsu, China). mRNA was then isolated from the total RNA using poly-T oligo-attached magnetic beads. For the construction of the RNA library, the purified mRNAs were cleaved into small fragments, first-strand cDNAs were produced by reverse transcription using a random hexamer primer and second-strand cDNAs are synthesized while simultaneously performing end repair and dA-Tailing. Sequencing adapter ligation was performed, followed by DNA magnetic bead purification and fragment selection after ligation was completed to yield a library with 250-350 bp insert fragments. The ligated products were amplified by PCR and purified again using DNA magnetic beads. After the initial library was constructed, a Qubit fluorescence quantifier was used for concentration detection, followed by a Qsep400 high-throughput biofragment analyzer for fragment size detection. The prepared library was sequenced on an Illumina platform.

2.6 RNA-Seq Data Analysis

The raw data were filtered using fastp (v 0.23.2) and generated clean reads to ensure the data's suitability for further analysis. Transcriptome assembly of clean reads was performed using Trinity (v 2.15.1), and the assembled transcripts were clustered and de-redundant using Corset (v 1.09). TransDecoder (v 5.3.0) was used to perform CDS prediction of Trinity assembled transcripts to obtain the corresponding amino acid sequences. Transcript sequences after de-redundancy were aligned with KEGG, NR, Swiss-Prot, GO, COG/KOG, and Trembl databases using DIAMOND software (v 2.0.9). The expression level of transcripts was calculated using RSEM software (v 1.3.1), and then the Fragments Per Kilobase of transcript per Million (FPKM) of each transcript was calculated according to the transcript length. Differentially expressed genes (DEGs) were rigorously identified based on a threshold of false discovery rate (FDR) < 0.05 and an absolute log2 fold change greater than 1 by DESeq2 software (v 1.22.2). Advanced analyses included GO enrichment, which dissected the biological processes (BP), cellular components (CC) and molecular functions (MF) associated with the DEGs. KEGG pathway enrichment analysis was then performed to elucidate the biological pathways engaged by these genes.

2.7 Metabolomic analysis

The samples were dried using a vacuum freeze dryer (Scientz-100F), 1200 μL of -20 °C pre-cooled 70 % methanolic aqueous internal standard extract were added to 50 mg of sample powder. Vortex once every 30 min for 30 sec, for a total of 6 times. After 12000 rpm, 3 min centrifugation, the supernatant was aspirated, and the sample was filtered through a 0.22 μm microporous membrane and stored in the injection vial for UPLC-MS/MS analysis. The sample extracts were analyzed using an UPLC-ESI-MS/MS system (UPLC, ExionLC™ AD, https: //sciex.com.cn/) and Tandem mass spectrometry system (https://sciex.com.cn/). The analytical conditions were used as Lv's method (Lv et al., 2024). Principal component analysis (PCA) was performed by statistical function "prcomp" within R (www.r-project.org). The HCA (hierarchical cluster analysis) results of samples and metabolites were presented as heatmaps

with dendrograms, while Pearson correlation coefficients (PCC) between samples were calculated by the “cor” function in R. Both HCA and PCC were carried out by R package Complex Heatmap. To identify differentially expressed metabolites (DEMs) between the groups, partial least squares-discriminant analysis (PLS-DA) was performed using the ‘ropls’ package in R (https://www.r-project.org/). DEMs were determined by VIP (VIP>1) and absolute Log2FC (|Log2FC|≥1.0). VIP values were extracted from OPLS-DA result, and was generated using R package MetaboAnalystR. Identified metabolites were annotated using KEGG Compound database (http://www.kegg.jp/kegg/ compound/), annotated metabolites were then mapped to KEGG Pathway database (http://www.kegg.jp/ kegg/pathway.html). The integrated analysis of the transcriptome and metabolome was performed after transforming their respective data into log2 values. To identify significant correlations between metabolites and genes within this combined analysis, Pearson's correlation coefficients greater than 0.8 and p-values less than 0.05 were utilized. For the analysis, co-annotated KEGG pathways with a q-value less than 0.05 were employed to assess the relationships between changes in gene expression and metabolite levels, adopting a simplified modular approach from classical KEGG pathways to illustrate these significant changes.

2.8 Soil DNA Extraction and Accu16S and AccuITS Sequencing Sequencing

Soil microbial DNA was extracted from 0.5 g of soil from each of the three replicates using the PowerSoil DNA Isolation Kit (Qiagen, Hilden, Germany), adhering to the manufacturer's instructions. The DNA's purity and quality were verified through PCR amplification and 2 % agarose gel electrophoresis. Subsequently, 16S and ITS amplicon libraries were constructed and sequenced, and the resulting reads along with the absolute copy numbers of the spike-in standards' 16S and ITS amplicons were used to create a standard curve. This curve was used to determine the absolute copy numbers of 16S and ITS rRNA genes for species falling within the standard curve's range in the sample. Specific primers targeting the bacterial 16S rDNA (V4 + V5) regions and fungal ITS sequences with primers ITS1F and ITS2R were employed for PCR amplification. A concentration of 10 ng/μL of sample DNA and spike-in internal reference DNA served as templates in the PCR system. Each sample was spiked with suitable internal reference DNA to amplify targeted regions, and positive control samples were prepared. A unique tag sequence was introduced at the end of each library using a primer with an Index sequence during high-fidelity PCR, allowing for the mixing of multiple samples in subsequent sequencing stages and enabling sample differentiation in bioinformatic analyses based on unique label sequences. After preliminary agarose gel electrophoresis, the concentrations of the sample libraries were appropriately diluted. The libraries were then precisely quantified using Qubit, and the ABI 3730 device was used to measure the insert size in the sequencing library, confirming the absence of nonspecific amplification between 120 and 200 bp and accurately determining the library concentration. Sequencing was performed using an Illumina 2 × 250 bp paired-end sequencing approach, followed by bioinformatics analysis to interpret the data.

3. Results

3.1 Comparative Analysis of Alkaloid Content in *L. radiata* Across Different Regions in China

L. radiata is highly valued as its robust biosynthesis of medicinal alkaloids especially galanthamine, lycorine and lycorenine. We investigated the community distribution of *L. radiata* across 11 major provinces in China, and found significant differences (~81.57 fold) in Gal content among different provinces (Figure 1A). The Gal content of *L. radiata* in Hubei Province was the highest, with a content of 552.65 μg/g DW, while it in Guangxi Province is the lowest, with a content of 6.77 μg/g DW (Figure 1B). Large differences (~6.76 fold) could be observed in Lycm contents among different provinces, the samples in Sichuan and Hubei Province had high Lycm contents, with a content of 759.60 μg/g DW and 738.96μg/g DW, while the samples in Yunnan Province are the lowest (112.36 μg/g DW). Compared with Gal and Lycm, there is a little difference (~2.29 fold) in the content of Lyc among different provinces, *L. radiata* resources in Guangxi Province are the highest (2689.79 μg/g DW), and in Shandong Province are the lowest (1172.21 μg/g DW) (Figure 1B).

To understand if the metabolomic profiles of *L. radiata* from different regions also exhibit a region-specific manner besides the target alkaloids (Gal, Lycm, Lyc), we selected Xingshan County in Yichang City, Hubei Province (HB group), which had high Gal and Lycm contents, middle Lyc content, Zhenxiong County in Zhaotong City, Yunnan Province (YN group) which had middle Gal, low Lycm and Lyc content, and Dumo County in Guilin City, Guangxi Province (GX group) which has a low Gal, middle Lycm, high Lyc content, for comparative study. We performed untargeted metabolomic analysis of the HB, GX, and YN populations. PCA analysis revealed robust clustering of biological replicates and distinct separation among the three geographical regions (Figure S1A). Pearson's correlation matrixes further validated the high reproducibility within groups and structural divergence between regions (Figure S1B). When comparing the differentially accumulated metabolites (DAMs) of GX to that of YN, 1360 DAMs were significantly down-regulated while 393 DAMs were up-regulated in GX, indicating a richer metabolome of YN (Figure 2A). A similar trend was observed when comparing HB to YN, with 1345 DAMs showing lower accumulation while 393 DAMs showing higher accumulation in HB. When comparing HB to GX, 843 DAMs showed higher accumulation while 749 showed lower accumulation. To pinpoint the primary metabolic drivers of these regional differences, we evaluated the top DAMs based on Variable Importance in Projection (VIP) scores from OPLS-DA models (Figure 2B-D). Only 2 metabolites in the top VIP metabolites when comparing GX to YN were more accumulated in GX and 3 alkaloids, tazettadoil, vittatine acetate and sinapoylputrescine were identified among eighteen metabolites that were more accumulated in YN. Two alkaloids (8-Demethoxyhostasine and 1-O-Acetylnorpluviine) and one quinone(5-hydroxy-anthraquinone-2-carboxylic acid) showed higher content in HB while 17 metabolites showing lower content in HB. When comparing HB with GX, 13 metabolites were more accumulated in HB including 5 alkaloids while 7 metabolites were less accumulated in HB. Further analysis of metabolite classes of DAMs showed similar results that apart from the differences in alkaloids, many flavonoids, lignans and coumarins, organic acids and quinones and lipids accumulated differently in 3 regions (Figure S2).

To specifically understand how the Amaryllidaceae alkaloid pathway is partitioned across these regions, we mapped the relative abundances of all detected alkaloid sub-classes. Our analysis revealed a highly diverse alkaloid profile (Figure 2E). Crucially, hierarchical clustering of these alkaloids demonstrated that

they do not accumulate in a same manner across all three regions. Instead, they are partitioned into distinct, region-specific accumulation clusters. For example, specific metabolites like Lycorine belong to a cluster heavily enriched in GX, whereas Galanthamine belongs to a cluster specifically enriched in HB. These results reveal the amaryllidaceae alkaloid biosynthesis exhibits significant regional differentiation. Key active components such as lycorine and galanthamine show specific accumulation patterns in different regions.

3.2 Transcriptional Profiling Reveals a Regional Paradox in Alkaloid Biosynthesis

To elucidate the underlying molecular mechanisms driving the spatial variation of alkaloids in *L. radiata*, we performed comparative transcriptomic analysis (RNA-seq) on the three representative populations (HB, YN, and GX). Principal Component Analysis (PCA) showed that samples from three regions exhibited distinct transcriptomic profiles and three biological replicates were nicely clustered within the regions (Figure S1C, 1D). We further identified differentially expressed genes (DEGs) by performing pairwise comparisons among transcriptomes of HB, GX, and YN (Figure S3). A core set of 4,392 DEGs was shared across all three pairwise comparisons indicating common regulatory responses. The comparison between HB and YN yielded the fewest total DEGs compared to comparisons involving GX (Figure S3A). The largest intersection consisted of 9,251 genes that were simultaneously down-regulated in both the GX_vs_YN and HB_vs_YN comparisons (Figure S3B). KEGG analysis on DEGs showed that “metabolic pathways” was the most enriched category in all comparison (Figure S4), which is in line with the divergent metabolic profiles of *L. radiata* from three regions.

The Gene Ontology (GO) term “alkaloid metabolic process” was significantly enriched exclusively in the GX_vs_YN and HB_vs_YN comparisons in GO enrichment analysis on the DEGs of pairwise comparisons of the three regions (Figure 3A). It indicates that the transcriptional regulation of alkaloid pathways in YN population diverges significantly from HB and GX. Among all DEGs enriched in the term “alkaloid metabolic process”, DEG numbers in GX_vs_YN and HB_vs_YN are 109 and 102 while it is only 91 in HB_vs_GX (Figure 3B). The expression profiles of these DEGs analyzed by hierarchical clustering exhibited distinct, region-specific manners and were therefore grouped into four major expression patterns (Figure 3C). Alkaloid biosynthesis is a complex enzymatic process, we hypothesized that the distinct accumulation patterns of Gal, Lycm and Lyc across these geographical regions might be governed by the differential transcription of key biosynthetic genes. Therefore, we mapped the expression levels of the key enzymes in biosynthesis of Gal, Lycm, and Lyc (Figure 4). Surprisingly, most of these core biosynthetic genes, including C*YP96T6*, *CYP96T5*, *SDR1*, *CYP96T1*, *C3H*, *PAL3*, and *C4H*, belonged predominantly to Cluster 2, where genes characterized by high expression in YN and relatively low transcription in HB and GX (Figure 3C), while a few exceptions existed, such as *TYDC* (Cluster 1, peaking in GX) and *OMT* (Cluster 3, maintained high in HB and YN). This transcriptional upregulation of key enzymes in YN suggests the YN population exhibits the highest transcriptomic potential for synthesizing Gal, Lycm, and Lyc, yet metabolomic profiling revealed that YN contained middle-to-low content of these specific alkaloids compared to HB and GX. This inconsistency suggests that the final

accumulation of these compounds is not strictly regulated at transcriptional level but may instead be subjected to regulations at post-transcriptional level or by environmental factors.

3.3 Rhizosphere Bacterial Communities Exhibits Regional Divergence

The rhizosphere microbiomes and local soil conditions are well-documented to act as crucial external stimulus, deeply involved in plant secondary metabolite biosynthesis and ecotypic divergence. To characterize the role of environments acting on *L. radiata* populations, we first performed 16S rRNA gene amplicon sequencing to profile the rhizosphere bacterial communities in HB, GX, and YN. Analysis of alpha diversity indicated by Shannon index revealed stark environmental disparities in microbial community structure (Figure 5A). The bacterial diversity in the YN rhizosphere was the lowest among three regions, suggesting that YN environment exhibits a highly specialized, less diverse microbial community. This regional distinctness was further revealed by beta diversity analyses. Principal Coordinates Analysis (PCoA) based on Bray-Curtis distances demonstrated that the bacterial communities strongly clustered by geographic origin, with the primary axis (PCoA1: 69.35%) driving a massive separation between the YN soil microbiome and those of HB and GX (Figure 5B). Venn diagram analysis at the Amplicon Sequence Variant (ASV) level showed minimal overlap, with only 9 ASVs shared universally across the three regions while the vast majority of ASVs were unique to their specific regions, underscoring that these ecotypes of *L. radiata* are exposed to fundamentally different microbial landscapes (Figure S5A). Moreover, there is little overlap when comparing YN with HB (12 ASVs) and GX (19 ASVs), while HB and GX had 119 ASVs in common, underscoring the fundamental taxonomic divergence of YN compared to that of HB and GX. To characterize the taxonomic architecture of these distinct regions, we analyzed the relative abundance of major bacterial genera. The taxonomic composition in YN was heavily dominated by a few genera such as *Acidothermus* and *Conexibacter*, which explains its low Shannon index (Figure 5C). Differential abundance analysis showed that genera such as *Conexibacter* and *Bradyrhizobium* were massively enriched in the YN rhizosphere compared to both HB and GX (Figure 5D, E, F). Hierarchical clustering of these differentially abundant genera further confirmed that the soil microbiota is tightly structured according to geographic origin (Figure S5B). To further investigate the microbial hub taxa defining these diverse soil environments, we performed Linear Discriminant Analysis Effect Size (LEfSe) analysis (Figure 5G). HB rhizosphere was structured by a broad array of distinguishing taxa, including *Gaiella*, *Solirubrobacter*, *Microvirga*, *Pedomicrobium* and *Pseudomonas*. *Conexibacter*, *Bradyrhizobium*, *Puia* and *Mucilaginibacter* are the dominant microbial hubs defining the YN soil bacterial communities whereas *Nitrospira* is identified as the biomarker of GX. Collectively, these data demonstrate that the *L. radiata* populations in HB, GX, and YN reside in different microbiological environments. The highly specialized, low-diversity bacterial community found in YN may provide a compelling environmental context for the divergent transcriptomic and metabolomic profiles observed in this specific population.

We further utilized ITS amplicon sequencing to characterize the fungal assemblies in the HB, GX, and YN rhizospheres. Consistent with the bacterial profiles, alpha diversity analysis of the fungal communities indicated by Shannon index revealed that the YN rhizosphere possessed a much lower fungal diversity

compared to the HB and GX (Figure 6A). This congruent cross-kingdom reduction in diversity may indicate that the YN ecosystem exerts intense environmental filtering, restricting community assembly to a highly specialized, ecotype-specific consortium. Beta diversity analysis further highlighted this strict geographic partitioning. PCoA demonstrated robust and complete separation of the fungal communities based on their geographic origins, with PCoA1 and PCoA2 accounting for 52.6 % and 42.58 % of the structural variance, respectively (Figure 6B). Moreover, the analysis at the ASV level identified a remarkably small cluster of cores mycobiome consisting of merely 33 shared ASVs, whereas hundreds of unique ASVs were specifically recruited by each distinct regional population (Figure S6A).To elucidate the taxonomic identities of these specific fungal interactors, we analyzed the differential abundance of major fungal genera. Hierarchical clustering revealed distinct, region-specific modules of fungal taxa that strictly co-associated with their respective host environments (Figure S6B). Pairwise differential abundance analyses further confirmed sweeping shifts in the dominant fungal populations across the three ecotypes (Figure 6C–E). To pinpoint the biomarkers driving these unique mycobiome networks, we applied LEfSe analysis (Figure 6F). YN soil was significantly characterized by the fungal hubs *Derxomyces*, *Hypomyces*, and *Podila*. HB ecotype selectively recruited a highly specific consortium dominated by *Fusarium* and *Aspergillus*. The GX soil was characterized by *Schizothecium*, *Linnemannia*, and *Penicillium*. Taken together, these cross-kingdom multi-omics data demonstrate that the *L. radiata* populations in HB, GX, and YN do not merely grow in different soils; they assemble drastically different holobionts. The localized recruitment of distinct bacterial and fungal elicitors acts as a complex, ecotype-specific environmental stimulus. This profound micro-ecological divergence provides the critical biological context necessary to explain why the observed transcriptomic activity in the plant diverts into widely varying downstream alkaloid profiles across different geographic regions.

3.4 Integrative Multi-Omics Analysis Reveals Distinct Drivers for Transcriptional Activation and Metabolite Accumulation

To investigate whether specific soil properties assemble the local microbiome and differentially tune the plant's gene-to-metabolite flux, we quantified 32 physicochemical soil indices and integrated them with our multi-omics datasets using Mantel tests. We observed profound environmental divergence across the three regions (Figure 7A). The soil in HB was a highly alkaline, mineral-dense environment with the highest relative levels of pH, Calcium (Ca), Magnesium (Mg), Sodium (Na), Aluminum (Al), Sulfur (S), and Barium (Ba), while being distinctly deficient in core organics and macronutrients (lowest content for OC, OM, TP, TN, and AN). In contrast, the GX soil was characterized by high Electrical Conductivity (EC) and peak levels of nitrogenous nutrients (TN, AN), Zinc (Zn), and Lead (Pb). The YN soil was defined as an acidic, highly hydrated environment under higher trace-metal load. The YN soil exhibited the lowest pH but possessed high relative concentrations of Water Content (WC) and almost all measured transition/heavy metals, including Iron (Fe), Manganese (Mn), Copper (Cu), Vanadium (V), Titanium (Ti), Cobalt (Co), Chromium (Cr), Nickel (Ni), and Strontium (Sr). Mantel test analyses demonstrated that both the bacterial and fungal communities exhibited highly robust correlations with an almost identical suite of soil indexes, which are trace metals and soil pH (Figure 7B, C), suggesting the soil environments may reshape or interact with bacterial and fungal communities in a similar way. The Gene Cluster 2 (C2)

which contains genes encoding most key biosynthesis enzymes of Amaryllidaceae alkaloids, correlated to distinct soil indexes with the Metabolite Clusters 2 and 4 (C2, C4), which harbor the Amaryllidaceae alkaloids(Figure 7D, 7E). Gene C2 was specifically elicited by water content and minerals such as Nickel (Ni), Bi, Sr, Fe, Cr and V and did not show significant correlation with bulk soil macronutrients (N, P, Organics). Metabolite C2 and C4 exhibited divergent environmental correlations (Figure 7E). Metabolite C2 lacked any highly significant primary environmental drivers, exhibiting only moderate correlations with a mixed array of indices including EC, TN, S, AN, Li, Zn, and Pb, while Metabolite C4 exhibited highly significant correlations with Total Phosphorus (TP), OC, OM, Na, Mg, Al and Ca. Taken together, the Mantel models revealed specific environmental factors that trigger gene transcription are uncoupled from the factors that may drive terminal metabolite accumulation.

4. Discussion

The spatial variation of secondary metabolites in medicinal plants is a complex phenomenon driven by a combination of genetic, environmental, and ecological factors. In this study, our comparative multi-omics analysis of *L. radiata* across distinct geographic regions (Hubei, Guangxi, and Yunnan) revealed highly localized metabolomic profiles. Most notably, we uncovered a transcriptional-metabolic paradox regarding Amaryllidaceae alkaloid biosynthesis: the Yunnan population exhibited the most robust transcriptional upregulation of core biosynthetic genes, yet it accumulated relatively lower concentrations of target alkaloids such as galanthamine and lycorine compared to the Hubei and Guangxi populations. This distinct uncoupling between genetic expression potential and the terminal chemical phenotype suggests that alkaloid accumulation in *L. radiata* is not governed solely by transcriptional regulation. Furthermore, our characterization of the rhizosphere microecology demonstrated that these regional host environments assemble drastically different, highly specialized bacterial and fungal microbiomes. By modeling these cross-kingdom multi-omics datasets alongside corresponding soil physicochemical properties, we observed that factors correlating with plant transcriptional activation (such as specific trace metals and water content) are largely uncoupled from the abiotic factors correlating with terminal metabolite accumulation (such as soil macronutrients and organic matter). Together, these findings highlight a profound ecotypic divergence in *L. radiata*, indicating that the localized environmental cues may trigger secondary metabolic pathways that differ significantly from those facilitating ultimate metabolite storage.

The biosynthesis of Amaryllidaceae alkaloids (e.g., galantamine and lycorine) originates from L-phenylalanine and L-tyrosine. The metabolic pathway depends on phenylalanine ammonia-lyase (PAL) and cytochrome P450 enzymes (particularly the CYP96T family), which are responsible for the key C–C phenol coupling reaction(Matthew B. Kilgore, Augustin, May, Crow, & Kutchan, 2016). The integrated analysis of metabolomics and transcriptomics led us to an interesting inconsistency. YN population possesses a massive upregulation of core alkaloid biosynthetic genes within gene cluster 2, specifically the *CYP96T* family and *PAL3* (Fig. 3, 4). However, metabolomic profiling uncovered a regional paradox where this high transcriptomic potential did not yield higher accumulation of targeted alkaloids. Instead, HB accumulated peak galanthamine and GX accumulated peak lycorine (Fig. 1, & 2E). Ultimately, the YN

metabolome was diverted into a significantly richer and more diverse profile of broad alkaloid derivatives rather than the hyper-accumulation of specific compounds (Fig. 2A &S2). This distinct "transcriptional-metabolic uncoupling" phenomenon indicates that high expression of key enzyme genes represents a highly activated biosynthetic pathway, but does not necessarily lead to substantial accumulation of a specific single end product. Previous study has failed to establish the positive correlation between transcriptional expression of galantamine biosynthesis genes and the actual content of galantamine. The researchers investigated galantamine content of root, bulb, and leaf samples of *L. radiata* found leaf samples had least accumulation of galantamine while bulb samples had the most accumulation. Further investigations on key enzymes showed divergent expression levels. *LrPAL2, LrPAL3, LrC4H2, LrTYDC2* exhibited highest expression in root samples while *LrNNR, LrN4OMT* exhibited higher expression in leaf than in root samples (Chang Ha Park et al., 2019). These results suggest that metabolism is not only governed by the biological pyramid from transcripts to proteins, and finally to metabolites and transcript abundance does not fully equate to the actual *in vivo* enzymatic activities(Stitt & Gibon, 2014). The terminal accumulation of complex secondary metabolites is heavily subjected to downstream regulatory mechanisms that do not exist at the mRNA level(Vogel & Marcotte, 2012). In plant stress biology, when plants face extreme abiotic stress, secondary metabolic flux often undergoes redirection. Instead of channeling precursors linearly into a single specific metabolite, plants disperse the metabolic flux to synthesize a broad range of structurally diverse derivatives, thereby building a more extensive chemical defense network(Isah, 2019; Obata & Fernie, 2012). The massive, paradoxical upregulation of the core alkaloid transcriptomic machinery (Gene Cluster 2) in the YN ecotype may be explained by the extreme localized edaphic conditions we characterized. Our soil profiling revealed that the YN environment is highly acidic and burdened with high content of minerals, including Iron (Fe), Chromium (Cr), Vanadium (V), Nickel (Ni), Copper (Cu), and Cobalt (Co), which are potential abiotic elicitors that expose plants to heavy metal stresses and oxidative stress. To survive this persistent stress, the plant acts according to the “cry-for-help” hypothesis(Rolfe, Griffiths, & Ton, 2019; Sasse et al., 2018), constitutively “turning on” its secondary metabolic defense networks (Asgari Lajayer, Ghorbanpour, & Nikabadi, 2017; Pascale, Proietti, Pantelides, & Stringlis, 2020). Our Mantel test models further validated this by showing that transcriptional activation was significantly correlated with specific metals (Ni, Bi, Sr, Fe, Cr, V) rather than bulk macronutrients (Fig. 7C). However, while trace-metal stress drives high gene expression, it paradoxically acts as a primary metabolic roadblock for alkaloid accumulation in YN populations. the uptake of heavy metals replaces essential cofactors of enzymes which hampers the metabolic functions (Mohamed et al., 2025). Heavy metals such as Nickel and Chromium are known to bind to thiol (-SH) groups in enzymes, leading to structural deformation and post-translational inactivation of biosynthetic proteins (Küpper & Andresen, 2016). Therefore, we suspect that heavy metals in YN soil elicit stress responses that up-regulates genes involved in secondary metabolite biosynthesis but inhibits enzymatic activities which lead to the inconsistency of gene expression and alkaloids accumulation. Therefore, we hypothesize that the high transcriptional activity but low alkaloid accumulation observed in the Yunnan population could be an adaptive strategy for metabolic resource reallocation in response to specific habitats.

The significant differences in soil physicochemical properties of the habitats, along with their strong filtering effect on rhizosphere microbial communities, can explain this metabolic flux redirection. Results from Mantel tests revealed a clear dissociation between the dominant factors determining rhizosphere microbial community assembly and key gene expression, and the environmental factors regulating the accumulation of terminal metabolites. The Yunnan habitat exhibits extreme characteristics, including strong acidity, high humidity, and high enrichment of heavy metals such as nickel, chromium, and strontium. This harsh soil environment exerts strong ecological selection pressure (environmental filtering), leading to a marked reduction in the diversity of the rhizosphere microecosystem of the Yunnan population and the selection of highly specialized, stress-tolerant core microbiota (e.g., *Acidothermus*). Previous studies have shown that heavy metal stress and specific symbiotic microbial molecular patterns (MAMPs) can act as potent elicitors, rapidly activating the plant's basal defense network and inducing large-scale expression of upstream secondary metabolism genes, including PAL and CYP96T(Yang et al., 2018). This explains the global upregulation of Gene Cluster 2 in the Yunnan population: it represents a stress-induced survival response to a harsh microecological environment.Despite the YN soil being deficient in available nitrogen compared to GX, our 16S sequencing revealed an enrichment of *Bradyrhizobium*, which is a well-documented microbial hub with high nitrogen-fixing capacity (Zhong et al., 2024). However, even if *Bradyrhizobium* supplies nitrogen, the accumulation of galantamine and lycorine is still low in YN. The biosynthesis of alkaloids requires a precise ratio of nitrogen (for the amine group) to carbon (for the phenolic scaffold) and phosphorus (for ATP-dependent enzymatic steps). While *Bradyrhizobium* resolves the nitrogen limitation in YN, the soil is severely deficient in organic carbon and phosphorus (Fig. 7A). The terminal steps of galanthamine biosynthesis, particularly those mediated by *OMT* and *NMT*, are S-adenosyl-L-methionine (SAM)-dependent and highly ATP-intensive (M. B. Kilgore et al., 2014; Mehta et al., 2024). The deficiency in phosphorus and carbon in YN creates a bottleneck that high nitrogen cannot overcome, stalling the metabolic flux and resulting in low alkaloid accumulation. Consistently, we observed strong positive correlation of metabolite cluster 4 with total phosphorus and organic carbon (Fig. 7E).

In contrast to the stalled flux in YN, the HB ecotype successfully hyper-accumulates galanthamine. The HB rhizosphere was dominated by *Fusarium* and *Aspergillus* (Fig. 6D), which are soil phytopathogens producing mycotoxins which leads to great economic losses of crop plants (Todorovic, Moenne-Loccoz, Raicevic, Jovicic-Petrovic, & Muller, 2023; Zakaria, 2024). Fungal elicitors activate highly specific signal transduction pathways that directly upregulate the terminal enzymes of secondary metabolic networks (Zhao, Davis, & Verpoorte, 2005). The specific biotic pressure in YN may force the available transcriptomic precursors toward the complete, terminal biosynthesis of specific defensive toxins like galanthamine.

Conclusion

Our study demonstrated significant spatial differentiation in the accumulation of key medicinal alkaloids in *Lycoris radiata*, including galanthamine, lycorine, and lycoramine, with differences in content reaching up to 80-fold across provinces. Through comparative multi-omics analysis, we identified high

transcriptional activity of core alkaloid biosynthetic genes in the Yunnan population which did not translate into high metabolite accumulation. This indicates that the final chemical phenotype of *L. radiata* is not strictly governed by transcriptional regulation but likely involves post-transcriptional mechanisms or environmental limitations on storage. Furthermore, our analysis of the rhizosphere microbiomes revealed that regional populations assemble fundamentally different bacterial and fungal landscapes, with the Yunnan rhizosphere exhibiting highly specialized, low-diversity microbial communities. The integration of soil physicochemical properties with these multi-omics datasets suggests that the local environment plays a dual role: while soil pH and trace metals are strongly associated with microbiome assembly, the factors triggering biosynthetic gene expression (such as water content and heavy metals) appear to be uncoupled from those associated with terminal metabolite accumulation (such as soil organic matter and phosphorus). Collectively, these findings highlight the complex micro-ecological and molecular divergence of *L. radiata* ecotypes. This study provides a detailed framework for understanding how localized environmental cues and distinct holobiont assemblies contribute to the chemical variability of this valuable medicinal resource.

Abbreviations

AN: Available nitrogen;

ASV: Amplicon sequence variant

BP: Biological process

CC: Cellular component

DAM: Differentially accumulated metabolite

DEG: Differentially expressed gene

DNA: Deoxyribonucleic acid

EC: Electrical conductivity

FDR: False discovery rate

FPKM: Fragments per kilobase of transcript per million mapped reads

Gal: Galanthamine

GO: Gene Ontology

GX: Guangxi

HB: Hubei

HCA: Hierarchical cluster analysis

ITS: Internal transcribed spacer

KEGG: Kyoto Encyclopedia of Genes and Genomes

LDA: Linear discriminant analysis

LEfSe: Linear discriminant analysis effect size

Lyc: Lycorine; Lycm: Lycoramine

MF: Molecular function

NCBI: National Center for Biotechnology Information

OC: Organic carbon

OM: Organic matter

OPLS-DA: Orthogonal partial least squares discriminant analysis

PCA: Principal component analysis

PCC: Pearson correlation coefficient

PCoA: Principal coordinates analysis

PCR: Polymerase chain reaction

RNA: Ribonucleic acid

RNA-seq: RNA sequencing

SRA: Sequence Read Archive

TK: Total potassium

TN: Total nitrogen

TP: Total phosphorus

UPLC-ESI-MS/MS: Ultra-performance liquid chromatography–electrospray ionization–tandem mass spectrometry

UPLC-MS/MS: Ultra-performance liquid chromatography–tandem mass spectrometry ***VIP:*** Variable importance in projection

WC: Water content

Declarations

Ethics approval and consent to participate

Not applicable.

Consent for publication

Not applicable.

Availability of data and materials

The datasets supporting the conclusions of this article are available in the NCBI database under BioProject ID: PRJNA1444724 and SRA ID: PRJNA1447745, unique persistent identifier and hyperlink to dataset(s) in http://www.ncbi.nlm.nih.gov/bioproject/1444724, https://www.ncbi.nlm.nih.gov/sra/PRJNA1447745. The metabolomics data, targeted alkaloid measurements, soil physicochemical data, and other datasets supporting the findings of this study are included in this article and its supplementary information files. Additional data are available from the corresponding authors upon reasonable request.

Competing Interest

The authors declare that they have no known competing financial interests or personal relationships that could have appeared to influence the work reported in this paper.

Authors' contributions

Q.Z.L. contributed to the original draft writing, visualization, formal analysis, conceptualization, data curation, and investigation. H.F.L. contributed to the original draft writing, formal analysis, data curation, methodology, and validation. S.Y.H. contributed to investigation, resources, and data curation. J.X.X., L.Z., Z.M.R. contributed to investigation and resources. Z.W. contributed to software, formal analysis, and visualization. Z.Y. contributed to data curation, supervision and validation. X.M.G. and Y.M.C.contributed to software, methodology, and formal analysis. F.Y.Z. contributed to writing, review and editing, project administration, and funding acquisition. L.Y.Y. contributed to writing, review and editing, supervision, funding acquisition, and conceptualization. Y.C.Z. contributed to writing, review and editing, supervision, project administration, funding acquisition, and conceptualization. All authors read and approved the final manuscript.

Funding

This work was supported by the Natural Science Foundation of Shanghai (25ZR1401315), the Shenzhen Science and Technology Program (JCYJ20240813145916021), the Natural Science Foundation of

Guangdong Province, China (2025A1515011598), Shanghai Rising-Star Program, China (No.20QB1404100), the National Natural Science Foundation of China (31801889, 32002067), the Shanghai Professional Technical Service Platform for Plant Seedling Tissue Culture (21DZ2292300) and the Shanghai Project Supported by the Central Funds Guiding Local Science and Technology Development (YDZX20223100003004).

Acknowledgements

We are deeply grateful to Professor Pengchong Zhang of Hangzhou Botanical Garden for his professional assistance in taxonomic verification. He carefully identified all wild plant samples and provided critical taxonomic references to support the accuracy of species information in this manuscript.

References

1. Asgari Lajayer B, Ghorbanpour M, Nikabadi S. Heavy metals in contaminated environment: Destiny of secondary metabolite biosynthesis, oxidative status and phytoextraction in medicinal plants. Ecotoxicol Environ Saf. 2017;145:377–90. https://doi.org/10.1016/j.ecoenv.2017.07.035.
2. Borges CV, Minatel IO, Gomez-Gomez HA, Lima GPP. Medicinal Plants: Influence of Environmental Factors on the Content of Secondary Metabolites. In: Ghorbanpour M, Varma A, editors. Medicinal Plants and Environmental Challenges. Cham: Springer International Publishing; 2017. pp. 259–77.
3. Chen J-X, Zheng J, Cai Y-M, Xu J-X, Sun Y, Yang Z, Li Q-Z. (2025). Medicinal compounds and biotechnology of Amaryllidaceae alkaloids in Lycoris radiata. *Frontiers in Plant Science, Volume 16–2025*. 10.3389/fpls.2025.1639654
4. Curtis PD, Curtis GB, Miller WB. Relative Resistance of Ornamental Flowering Bulbs to Feeding Damage by Voles. HortTechnology. 2009;19(3):499–503. 10.21273/horttech.19.3.499.
5. Fernie AR, Stitt M. On the Discordance of Metabolomics with Proteomics and Transcriptomics: Coping with Increasing Complexity in Logic, Chemistry, and Network Interactions Scientific Correspondence. Plant Physiol. 2012;158(3):1139–45. 10.1104/pp.112.193235.
6. Isah T. (2019). Stress and defense responses in plant secondary metabolites production. Biol Res, 52.
7. Jiang X, Chen H, Wei X, Cai J. Proteomic analysis provides an insight into the molecular mechanism of development and flowering in Lycoris radiata. Acta Physiol Plant. 2021;43(1):4. 10.1007/s11738-020-03179-w.
8. Kilgore MB, Augustin MM, May GD, Crow JA, Kutchan TM. (2016). CYP96T1 of Narcissus sp. aff. pseudonarcissus Catalyzes Formation of the Para-Para' C-C Phenol Couple in the Amaryllidaceae Alkaloids. *Frontiers in Plant Science, Volume 7–2016*. 10.3389/fpls.2016.00225
9. Kilgore MB, Augustin MM, Starks CM, O'Neil-Johnson M, May GD, Crow JA, Kutchan TM. Cloning and characterization of a norbelladine 4'-O-methyltransferase involved in the biosynthesis of the

Alzheimer's drug galanthamine in Narcissus sp. aff. pseudonarcissus. PLoS ONE. 2014;9(7):e103223. 10.1371/journal.pone.0103223.

10. Kumari N, Manhas SK, Jose-Santhi J, Kalia D, Sheikh FR, Singh RK. Emerging into the world: regulation and control of dormancy and sprouting in geophytes. J Exp Bot. 2024;75(19):6125–41. 10.1093/jxb/erae216.
11. Küpper H, Andresen E. Mechanisms of metal toxicity in plants. Metallomics. 2016;8(3):269–85. 10.1039/c5mt00244c.
12. Liang J, Quan M, She C, He A, Xiang X, Cao F. Effects of drought stress on growth, photosynthesis and alkaloid accumulation of Lycoris aurea. Pak J Bot. 2020;52(4):5. 10.30848/PJB2020-4(15).
13. Liyanage NS, Awwad F, Gonçalves dos Santos KC, Jayawardena TU, Mérindol N, Desgagné-Penix I. Navigating Amaryllidaceae alkaloids: bridging gaps and charting biosynthetic territories. J Exp Bot. 2025;76(1):16–34. 10.1093/jxb/erae187.
14. Lombe BK, Zhou T, Kang G, Wood JC, Hamilton JP, Gase K, O'Connor SE. Biosynthesis of cinchona alkaloids. Nature. 2026. 10.1038/s41586-026-10227-x.
15. Mehta N, Meng Y, Zare R, Kamenetsky-Goldstein R, Sattely E. A developmental gradient reveals biosynthetic pathways to eukaryotic toxins in monocot geophytes. Cell. 2024;187(20):5620–e56375610. 10.1016/j.cell.2024.08.027.
16. Mohamed HI, Ullah I, Toor MD, Tanveer NA, Din MMU, Basit A, Rehman MU. Heavy metals toxicity in plants: understanding mechanisms and developing coping strategies for remediation: a review. Bioresources Bioprocess. 2025;12(1):95. 10.1186/s40643-025-00930-4.
17. Mucke HA. The case of galantamine: repurposing and late blooming of a cholinergic drug. Future Sci OA. 2015;1(4):Fso73. 10.4155/fso.15.73.
18. Nakayasu M, Ohno K, Takamatsu K, Aoki Y, Yamazaki S, Takase H, Sugiyama A. Tomato roots secrete tomatine to modulate the bacterial assemblage of the rhizosphere. Plant Physiol. 2021;186(1):270–84. 10.1093/plphys/kiab069.
19. Nakayasu M, Takamatsu K, Kanai K, Masuda S, Yamazaki S, Aoki Y, Sugiyama A. Tomato root-associated Sphingobium harbors genes for catabolizing toxic steroidal glycoalkaloids. mBio. 2023;14(5):e00599–00523. 10.1128/mbio.00599-23.
20. Obata T, Fernie AR. The use of metabolomics to dissect plant responses to abiotic stresses. Cell Mol Life Sci. 2012;69(19):3225–43.
21. Pang Z, Chen J, Wang T, Gao C, Li Z, Guo L, Cheng Y. (2021). Linking Plant Secondary Metabolites and Plant Microbiomes: A Review. *Frontiers in Plant Science, Volume 12–2021*. 10.3389/fpls.2021.621276
22. Park CH, Yeo HJ, Park YE, Baek S-A, Kim JK, Park SU. Transcriptome Analysis and Metabolic Profiling of Lycoris Radiata. Biology. 2019;8(3). 10.3390/biology8030063.
23. Park CH, Yeo HJ, Park YE, Baek S-A, Kim JK, Park SU. Transcriptome Analysis and Metabolic Profiling of Lycoris Radiata. Biology. 2019;8(3):63. 10.3390/biology8030063.

24. Pascale A, Proietti S, Pantelides IS, Stringlis IA. (2020). Modulation of the Root Microbiome by Plant Molecules: The Basis for Targeted Disease Suppression and Plant Growth Promotion. *Frontiers in Plant Science, Volume 10–2019*. 10.3389/fpls.2019.01741
25. Quan M, Jiang X, Xiao L, Li J, Liang J, Liu G. Reciprocal natural hybridization between Lycoris aurea and Lycoris radiata (Amaryllidaceae) identified by morphological, karyotypic and chloroplast genomic data. BMC Plant Biol. 2024;24(1):14. 10.1186/s12870-023-04681-2.
26. Rasmann S, Agrawal AA. In Defense of Roots: A Research Agenda for Studying Plant Resistance to Belowground Herbivory. Plant Physiol. 2008;146(3):875–80. 10.1104/pp.107.112045.
27. Ren Z-M, Zhang D, Jiao C, Li D-Q, Wu Y, Wang X-Y, Xia Y-P. Comparative transcriptome and metabolome analyses identified the mode of sucrose degradation as a metabolic marker for early vegetative propagation in bulbs of Lycoris. Plant J. 2022;112(1):115–34. https://doi.org/10.1111/tpj.15935.
28. Ren Z, Wang J, Huang N, Fu H, Liu B, Xia Y. (2026). Meiosis in bulbous flower species Lycoris: dances underground. *Frontiers in Plant Science, Volume 16–2025*. 10.3389/fpls.2025.1691599
29. Rolfe SA, Griffiths J, Ton J. Crying out for help with root exudates: adaptive mechanisms by which stressed plants assemble health-promoting soil microbiomes. Curr Opin Microbiol. 2019;49:73–82. https://doi.org/10.1016/j.mib.2019.10.003.
30. Sasse J, Martinoia E, Northen T. Feed Your Friends: Do Plant Exudates Shape the Root Microbiome? Trends Plant Sci. 2018;23(1):25–41. https://doi.org/10.1016/j.tplants.2017.09.003.
31. Shu X, Lu R, Heslop-Harrison P, Schwarzacher T, Wang Z, Qin Y, Zhang F. Unraveling the evolutionary complexity of Lycoris: Insights into chromosomal variation, genome size, and phylogenetic relationships. Plant Divers. 2025;47(6):931–43. https://doi.org/10.1016/j.pld.2025.06.010.
32. Stitt M, Gibon Y. Why measure enzyme activities in the era of systems biology? Trends Plant Sci. 2014;19(4):256–65. https://doi.org/10.1016/j.tplants.2013.11.003.
33. Tang M, Li C, Zhang C, Cai Y, Zhang Y, Yang L, Li K. SWATH-MS-Based Proteomics Reveals the Regulatory Metabolism of Amaryllidaceae Alkaloids in Three Lycoris Species. Int J Mol Sci. 2023;24(5):4495. 10.3390/ijms24054495.
34. Todorovic I, Moenne-Loccoz Y, Raicevic V, Jovicic-Petrovic J, Muller D. (2023). Microbial diversity in soils suppressive to diseases. *Frontiers in Plant Science, 14*. doi:ARTN 122874910.3389/fpls.2023.1228749.
35. Vogel C, Marcotte EM. Insights into the regulation of protein abundance from proteomic and transcriptomic analyses. Nat Rev Genet. 2012;13(4):227–32. 10.1038/nrg3185.
36. Yahyazadeh M, Meinen R, Hänsch R, Abouzeid S, Selmar D. Impact of drought and salt stress on the biosynthesis of alkaloids in Chelidonium majus L. Phytochemistry. 2018;152:204–12. https://doi.org/10.1016/j.phytochem.2018.05.007.
37. Yang L, Wen K-S, Ruan X, Zhao Y-X, Wei F, Wang Q. Response of plant secondary metabolites to environmental factors. Molecules. 2018;23(4):762.

38. Zakaria L. An Overview of Aspergillus Species Associated with Plant Diseases. Pathogens. 2024;13(9):813. 10.3390/pathogens13090813.
39. Zhao J, Davis LC, Verpoorte R. Elicitor signal transduction leading to production of plant secondary metabolites. Biotechnol Adv. 2005;23(4):283–333. https://doi.org/10.1016/j.biotechadv.2005.01.003.
40. Zhong C, Hu G, Hu C, Xu C, Zhang Z, Ning K. Comparative genomics analysis reveals genetic characteristics and nitrogen fixation profile of Bradyrhizobium. iScience. 2024;27(2):108948. https://doi.org/10.1016/j.isci.2024.108948.
41. Ziegler J, Facchini PJ. Alkaloid biosynthesis: metabolism and trafficking. Annu Rev Plant Biol. 2008;59:735–69. 10.1146/annurev.arplant.59.032607.092730.
42. Zuo YW, Quan MH, Liu GH, Zhang X, Long NN, You SQ, Deng HP. Multi-Omics Analysis Reveals Molecular Responses of Alkaloid Content Variations in Lycoris aurea Across Different Locations. Plant Cell Environ. 2024;48(2):953–64. 10.1111/pce.15187.

Figures

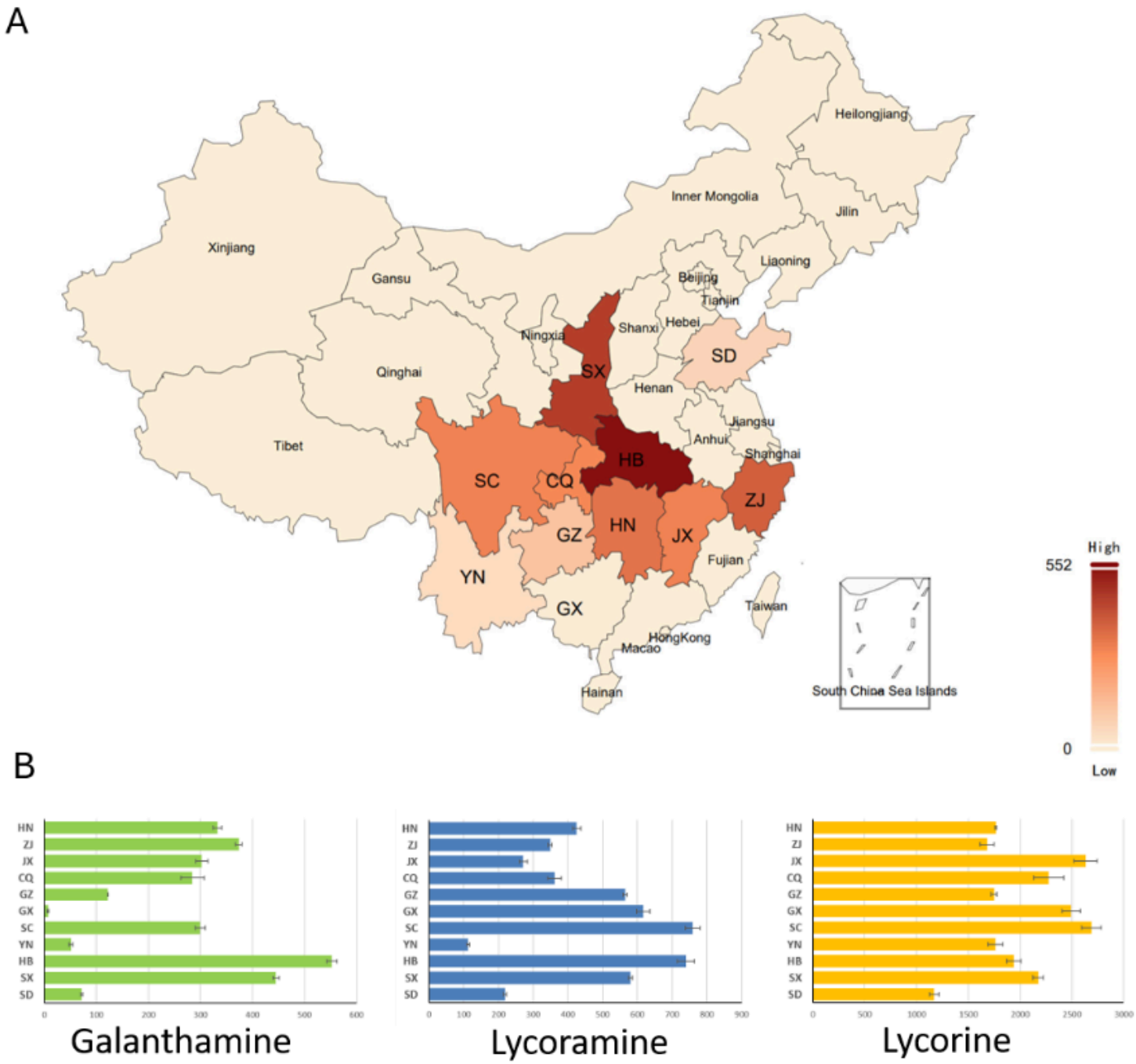


Figure 1

Geographic and biochemical analysis of *Lycoris radiata* across 11 provinces in China. A. Heatmap showing the concentrations of galanthamine in 11 provinces. SX(Shanxi), SD(Shandong), HB(Hubei), SC (Sichuan), CQ (Chongqing), HN (Hunan), YN (Yunnan), GZ (Guizhou), GX (Guangxi), JX (Jiangxi), ZJ (Zhejiang). B. Comparative analysis of galanthamine, lycoramine and lycorine contents measured by high-performance liquid chromatography in 11 provinces.

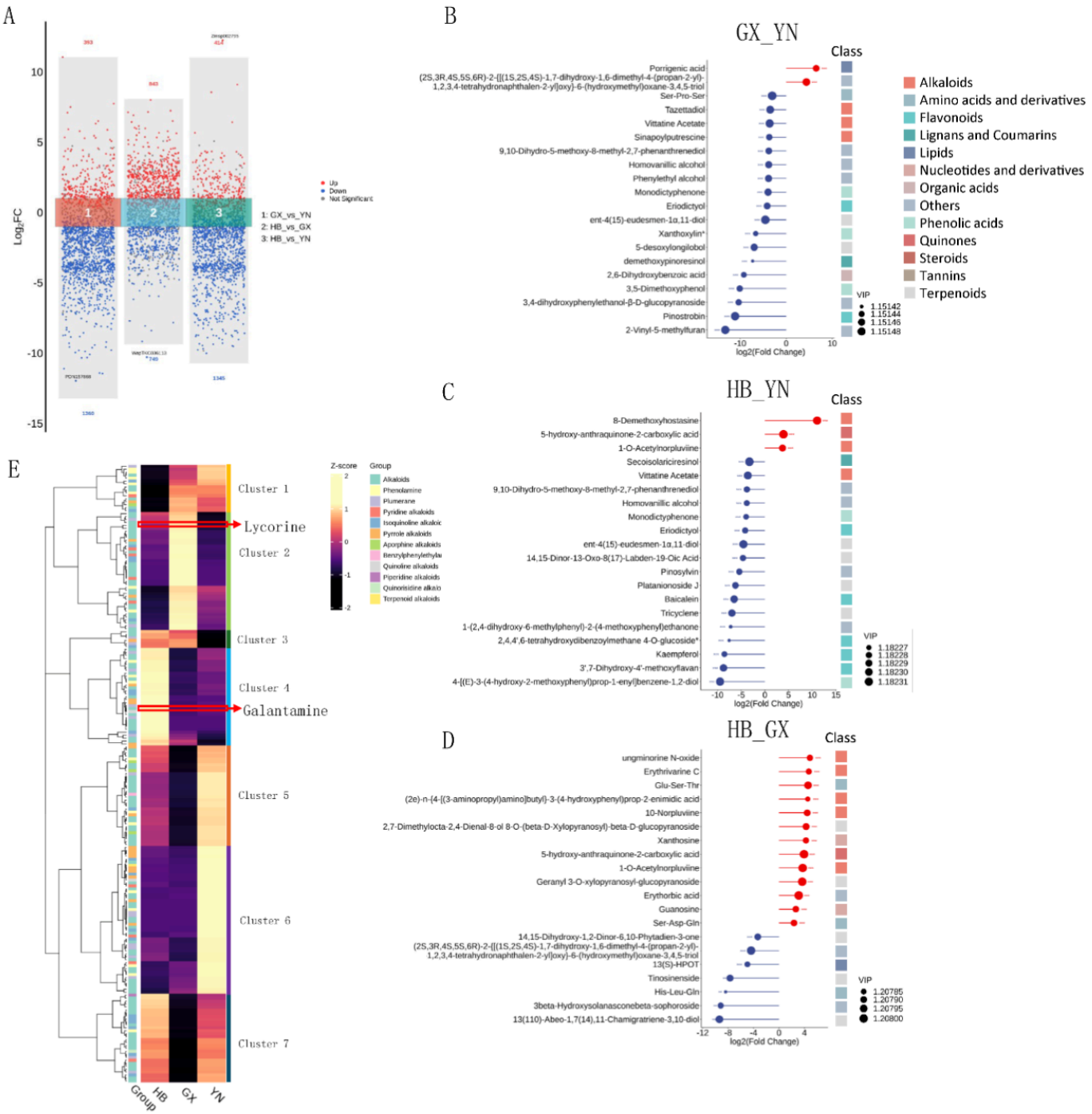


Figure 2

Lycoris radiata in Hubei, Guangxi and Yunan have divergent metabolic profiles. A. Up- and down-regulated metabolites in 3 groups. B-D. Metabolites evaluated with variable importance in projection (VIP) scores of OPLS-DA models when comparing metabolomes of Guangxi and Yunan(B), Hubei and Yunan(C), Hubei and Guangxi(D). The size of the dots indicates the VIP scores of the metabolites. The color of the dots indicates more (red) or less(blue) accumulation of the metabolite. The color of the blocks at the end of the chart indicates the classification of the metabolites. E. Galantamine and lycorine belong to region-specific clusters in the heatmap of differentially abundant metabolites in 3 places. HB, Hubei populations; GX, Guangxi populations; YN, Yunnan populations.

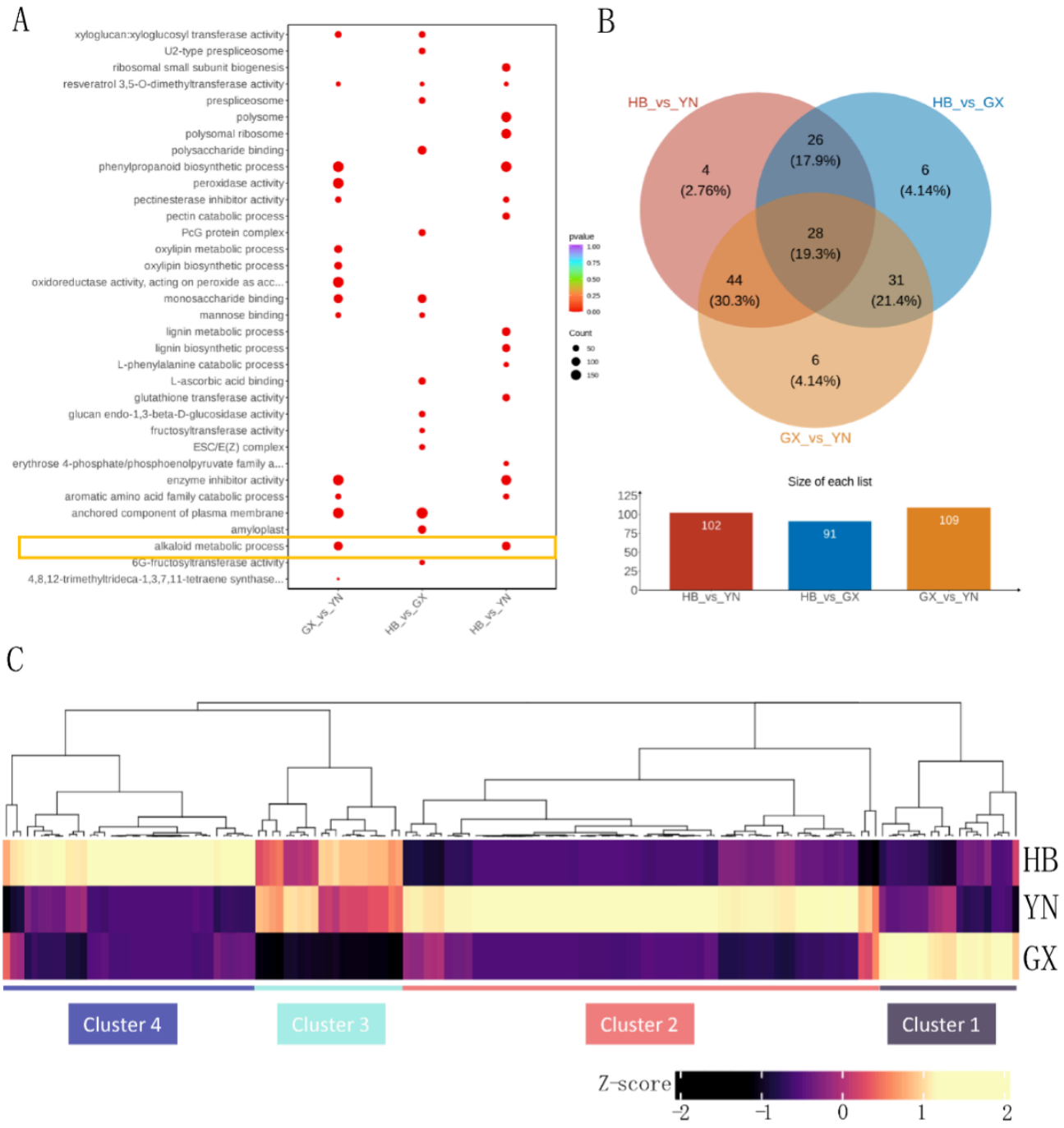


Figure 3

Genes involved in alkaloid biosynthesis are expressed in a region-specific manner. A. Alkaloid biosynthesis process was enriched in GO analysis on differentially expressed genes (DEGs) in three groups. These DEGs and their expression levels were shown in venn diagram (B) and clustered heatmap (C). HB, Hubei populations; GX, Guangxi populations; YN, Yunnan populations.

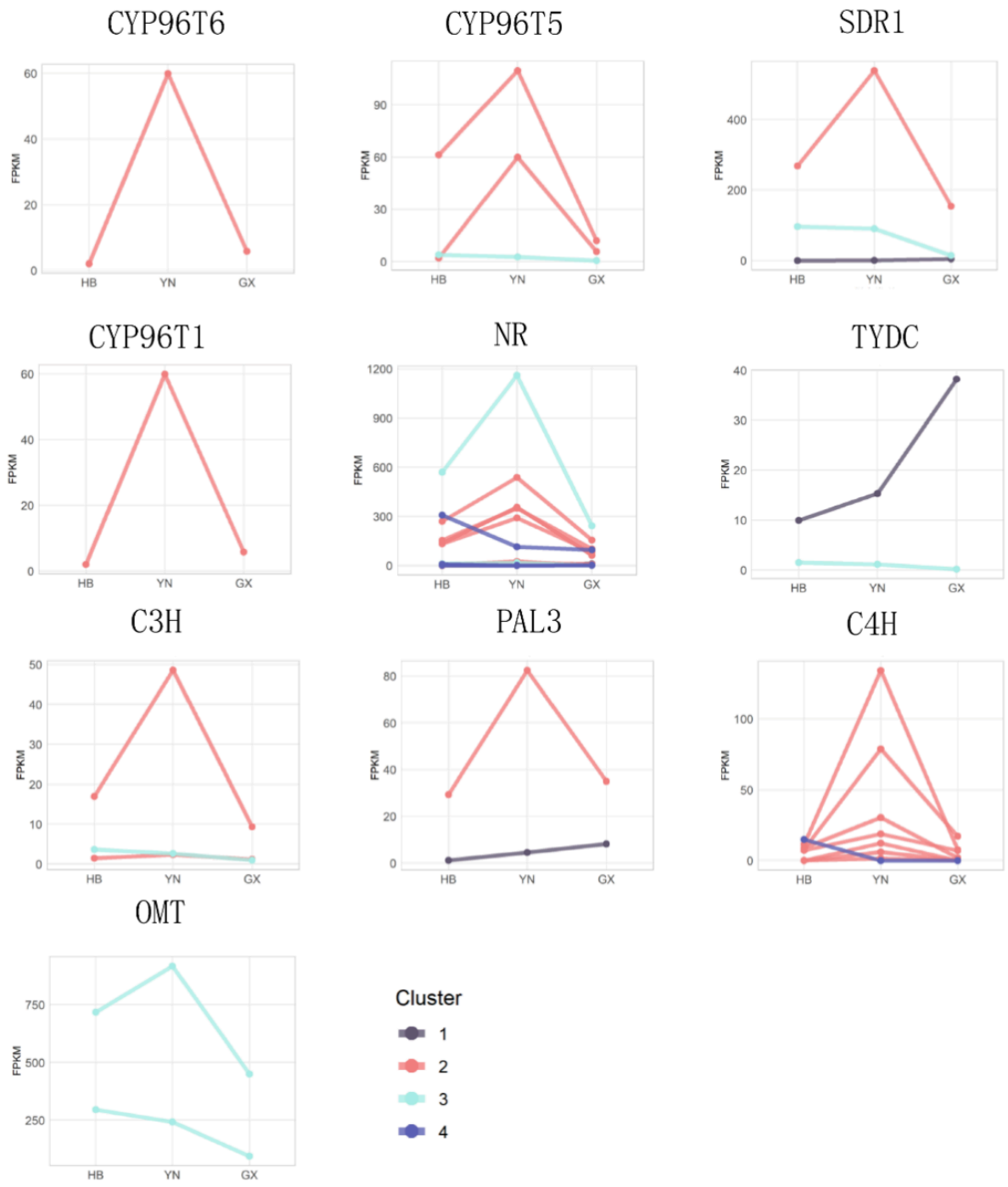


Figure 4

Expression patterns of DEGs enriched in biosynthesis pathways of galantamine, lycorine and lycoramine. The regional expressions of DEGs that were enriched in biosynthesis pathways of alkaloids and involved in biosynthesis of galantamine, lycorine and lycoramine were plotted. Colors indicate clusters from the heatmap in Figure 3C. HB, Hubei populations; GX, Guangxi populations; YN, Yunnan populations.

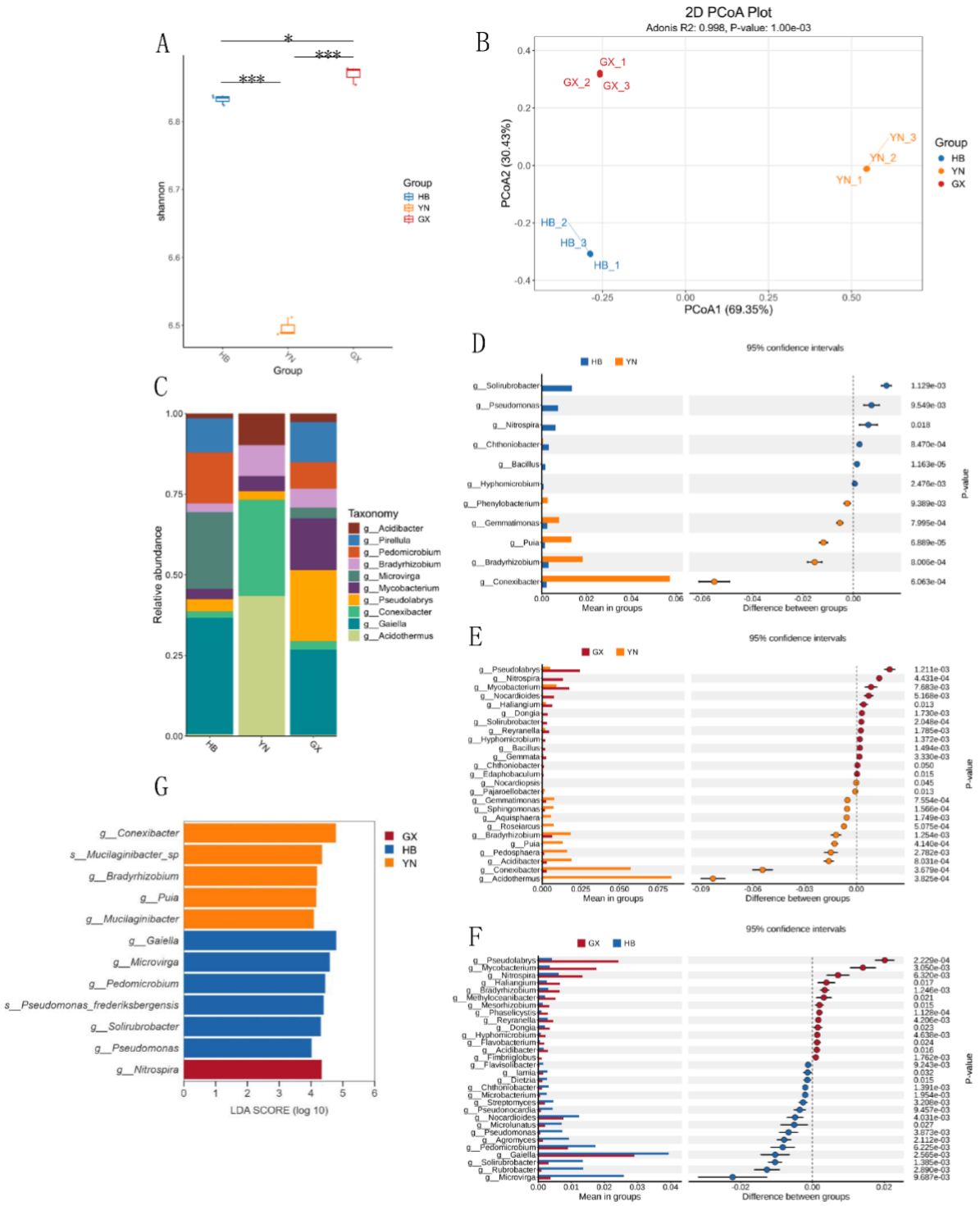


Figure 5

Bacterial community of rhizosphere soil in three places. A. Shannon index in samples from three places. B. Principal coordinates analysis (PCoA) performed based on Bray–Curtis distance matrices of bacterial communities derived from the soil microbiome samples of three places. C. The relative abundances of major (top 10) bacteria genera in the rhizosphere soil from three places. D-F. Differential abundant genera when compare every two places were characterized. The graph shows the relative abundance of

those genera in different places. G. Prediction of biomarker genera for three places by the linear discriminant analysis (LDA) effect size (LEfSe) analysis. Different colors indicate the places. HB, Hubei populations; GX, Guangxi populations; YN, Yunnan populations.

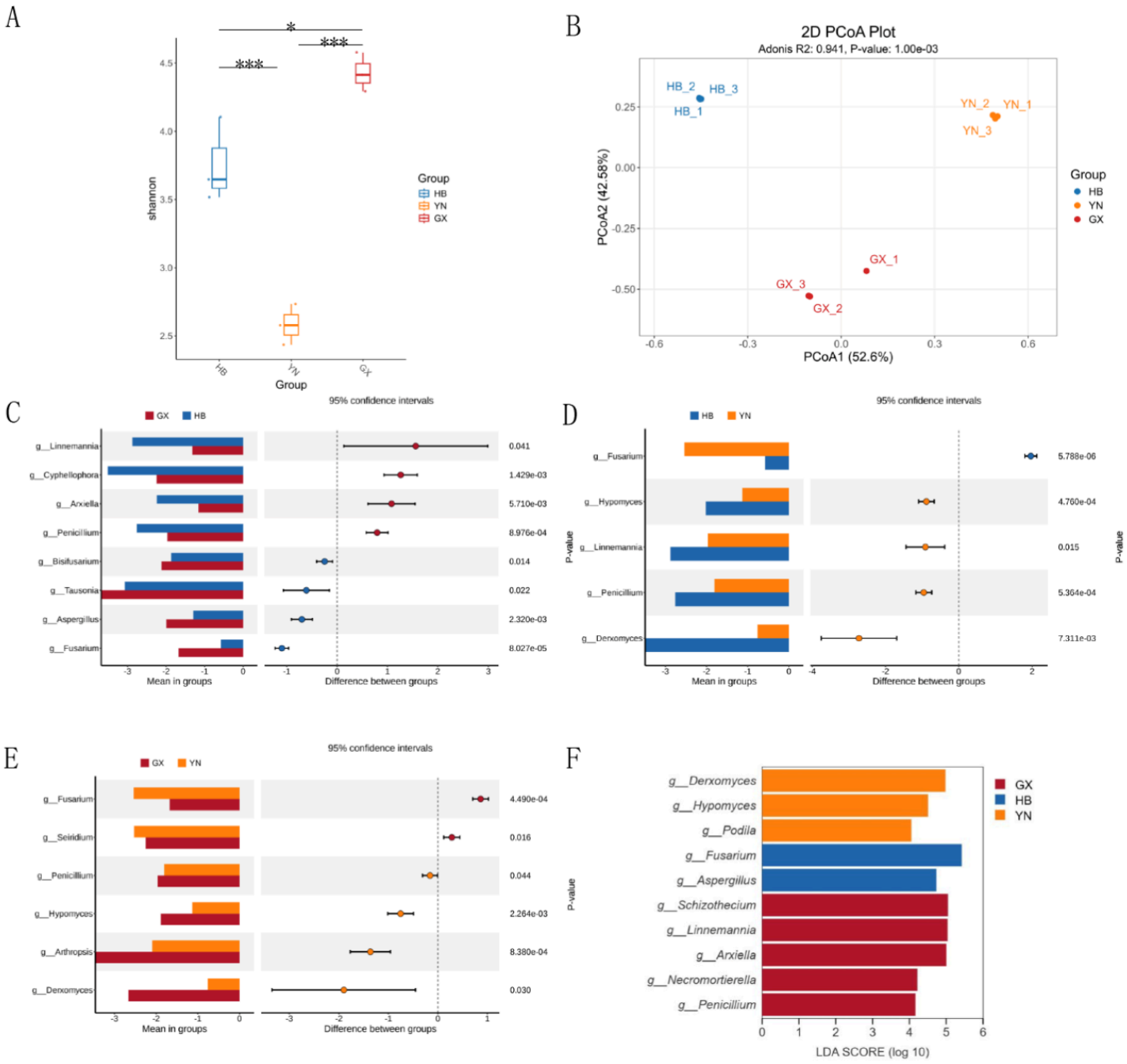


Figure 6

Fungal community of rhizosphere soil in three places. A. Shannon index in samples from three places. B. Principal coordinates analysis (PCoA) performed based on Bray–Curtis distance matrices of bacterial communities derived from the soil microbiome samples of three places. C-E. Differential abundant fungal genera when compare every two places were characterized. The graph shows the relative

abundance of those genera in different places. F. Prediction of biomarker genera for three places by the linear discriminant analysis (LDA) effect size (LEfSe) analysis. Different colors indicate the places. HB, Hubei populations; GX, Guangxi populations; YN, Yunnan populations.

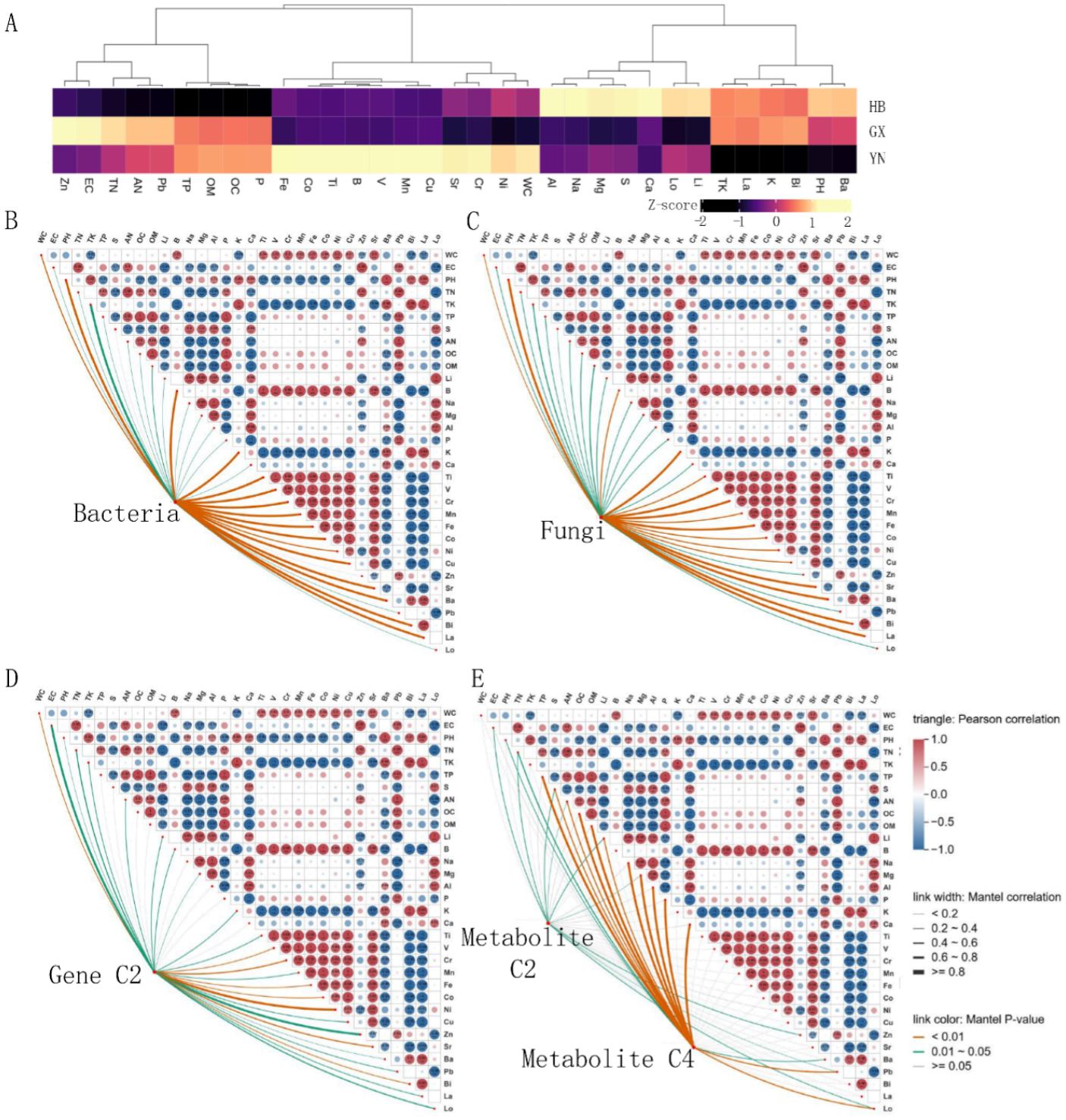


Figure 7

Relationships of gene, microbial communities with soil properties. A. Clustered heatmap of soil properties in three places. B-D. Mantel test analysis was conducted to explore correlations between bacteria (B), gene cluster 2 from Figure 2 (C), fungus(D) and metabolite cluster 2 and 4 from Figure 4(E) with soil properties. HB, Hubei populations; GX, Guangxi populations; YN, Yunnan populations.

Supplementary Files

This is a list of supplementary files associated with this preprint. Click to download.

- 0714SupplementaryMaterial.docx